Non-volatile ferroelectric control of ferromagnetism in (Ga,Mn)As

I. STOLICHNOV[1]*, S. W. E. RIESTER[1], H. J. TRODAHL[1,2], N. SETTER[1], A. W. RUSHFORTH[3], K. W. EDMONDS[3], R. P. CAMPION[3], C. T. FOXON[3], B. L. GALLAGHER[3] AND T. JUNGWIRTH[3,4]

[1]Ceramics Laboratory, EPFL-Swiss Federal Institute of Technology, Lausanne 1015, Switzerland
[2]MacDiarmid Institute for Advanced Materials and Nanotechnology, Victoria University, Wellington 6140, New Zealand
[3]School of Physics and Astronomy, University of Nottingham, Nottingham NG7 2RD, UK
[4]Institute of Physics ASCR v.v.i., Cukrovarnická 10, 162 53 Praha 6, Czech Republic
*e-mail: igor.stolitchnov@epfl.ch

Published online: 4 May 2008; doi:10.1038/nmat2185

Multiferroic structures that provide coupled ferroelectric and ferromagnetic responses are of significant interest as they may be used in novel memory devices and spintronic logic elements[1–4]. One approach towards this goal is the use of composites that couple ferromagnetic and ferroelectric layers through magnetostrictive and piezoelectric strain transmitted across the interfaces[5–7]. However, mechanical clamping of the films to the substrate limits their response[1,8]. Structures where the magnetic response is modulated directly by the electric field of the poled ferroelectric would eliminate this constraint and provide a qualitatively higher level of integration, combining the emerging field of multiferroics with conventional semiconductor microelectronics. Here, we report the realization of such a device using (Ga,Mn)As, which is an archetypical diluted magnetic semiconductor with well-understood carrier-mediated ferromagnetism, and a polymer ferroelectric gate. Polarization reversal of the gate by a single voltage pulse results in a persistent modulation of the Curie temperature of the ferromagnetic semiconductor. The non-volatile gating of (Ga,Mn)As has been made possible by applying a low-temperature copolymer deposition technique that is distinct from pre-existing technologies for ferroelectric gates on magnetic oxides. This accomplishment opens a way to nanometre-scale modulation of magnetic semiconductor properties with rewritable ferroelectric domain patterns, operating at modest voltages and subnanosecond times.

Non-volatile electric-field control of ferromagnetism using a ferroelectric gate has been reported in oxide ferromagnetic layers that do not lend themselves to integration with semiconductors. In particular, such control has been found in manganites[9] and Co-doped TiO_2 (ref. 10), although in the latter case it seems probable that the material is phase segregated and the ferromagnetism arises from Co clusters[11]. In contrast, here we use the well-established (Ga,Mn)As diluted magnetic semiconductor as the conducting channel in the ferroelectric-gate field-effect transistor (FeFET) structure, which offers close compatibility with its parent compound semiconductor GaAs. In this system, Mn substituting for Ga is an acceptor providing both local magnetic moments and valence band holes[12]. The control of ferromagnetism using the ferroelectric gate demonstrated here relies on the mediation of the Mn–Mn exchange interaction by the strongly spin–orbit coupled valence band holes that control the strength of the magnetic interactions, magnetocrystalline anisotropies and magnetotransport effects[12].

Volatile control of the magnetic response in a diluted magnetic semiconductor channel of a conventional FET was previously reported in magnetically doped group III–V, IV and II–VI semiconductors[13–18]. Here, the main focus is on the demonstration of persistent electrical control of ferromagnetism in terms of switching the collective magnetic state on and off, or equivalently, producing sizable changes in the Curie temperature.

Achieving a FeFET based on magnetic (Ga,Mn)As presents a number of challenges. The change in two-dimensional hole concentration that can be produced by a ferroelectric gate does not exceed the spontaneous polarization of the ferroelectric material, typically about 10 $\mu C\,cm^{-2}$ (6×10^{13} electrons cm^{-2}), and screening at the ferroelectric–semiconductor interface can reduce the induced charge below that ideal. The three-dimensional hole density in ferromagnetic (Ga,Mn)As is high (10^{20}–10^{21} cm^{-3} (10^{13}–10^{14} cm^{-2} per nanometre thickness)). The thinnest possible (Ga,Mn)As layers are therefore required. Thus, we have implemented our device with the thinnest (7 nm) layers of 6% Mn-doped GaAs that exhibit consistent and well-characterized ferromagnetic behaviour. A second challenge relates to an incompatibility between (Ga,Mn)As and the 400–600 °C anneal required for oxide ferroelectrics. A temperature much above 250 °C leads to a loss of substitutional Mn, reducing both the local moment density and the hole concentration on which the Mn–Mn exchange relies[19]. Thus, instead of a conventional perovskite ferroelectric, we have used a copolymer polyvinylidene fluoride with trifluoroethylene P(VDF-TrFE), which requires only a 140 °C anneal to align the polymer chains[20].

A cross-section of the FeFET structure is shown in Fig. 1. The 7 nm (Ga,Mn)As films were grown by low-temperature ($\leq$250 °C) molecular beam epitaxy onto a 330 nm high-temperature GaAs buffer layer on a semi-insulating GaAs (001) substrate. The uniaxial anisotropy with the easy magnetization axis parallel to the [1$\bar{1}$0] axis was confirmed by superconducting quantum interference device magnetometry, as reported earlier for similar films[21]. Two films were tested; film I shown in Fig. 1 was separated from the

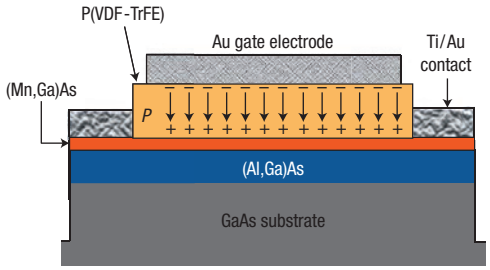

Figure 1 Schematic longitudinal cross-section of the Hall bar based on film I. The 7 nm Mn-doped layer is separated from the GaAs substrate by a (Ga,Al)As barrier. The top-to-bottom direction of the spontaneous polarization *P* in the ferroelectric gate corresponds to the depletion state.

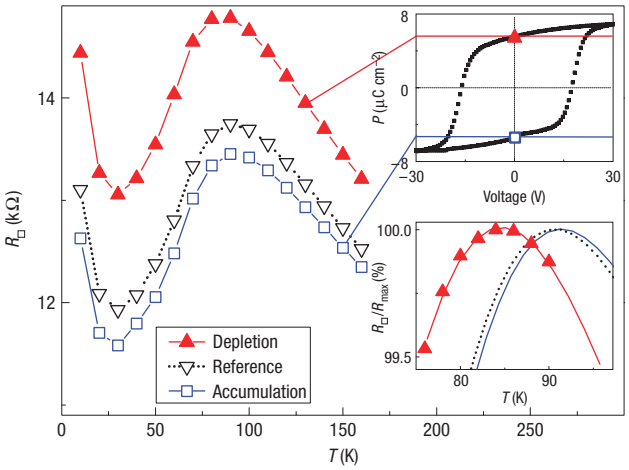

Figure 2 Ferroelectric gate operation and temperature dependence of the sheet resistance for film I. Hysteretic polarization reversal in the gate enables non-volatile switching between accumulation and depletion states. Around 80 K, the sheet resistance in the depleted state is 9% higher than in the accumulation state and the reference sample with ferroelectric gate removed lies in between. Upper inset: Polarization hysteresis loop of the gate driven with 1 kHz triangle pulse. Lower inset: Curves of resistance versus temperature normalized and zoomed in the region around the maximum occurring close to T_C. In the depletion state, the maximum shifts towards lower temperatures as expected.

buffer by a 50-nm-thick $Al_{0.33}Ga_{0.67}As$ barrier, whereas film II was deposited directly onto the buffer layer. Films I and II have room-temperature sheet resistances of 11 and 8 kΩ, respectively.

Hall bars of width 180 μm and length 2,300 μm were defined by chemical etching and Ti/Au (15 nm/125 nm) contacts were deposited by electron beam evaporation. The conducting channel was oriented parallel to the $[1\bar{1}0]$ crystal axis, corresponding to the easy magnetization axis. The 200 nm P(VDF-TrFE) ferroelectric gate polymer was spin-coated from the 2% methyl ethyl ketone solution and crystallized for 10 min at 137 °C. Finally, a 100 nm Au gate electrode was deposited by thermal evaporation.

The ferroelectric P(VDF-TrFE) films on (Ga,Mn)As show the sharp polarization hysteresis loop seen in the upper inset of Fig. 2, with an ambient-temperature remnant polarization close to 6 μC cm^{-2}. The polarization is stable for more than a week and after repeated cycling to 10 K, as confirmed by both polarization hysteresis and transverse piezoelectric response measured directly through the gate electrode by piezoelectric force microscopy[22] at room temperature. In our magnetotransport experiments, the gate was poled with a single +30 V (−30 V) voltage pulse.

Ferroelectric control of the hole density in the channel can be seen in Fig. 2, which compares the temperature-dependent resistivities of the channel in film I before and after poling the gate and a reference Hall bar with the ferroelectric gate removed. Polarizing the gate induces a resistivity change between accumulation and depletion of ∼4% at 300 K, ∼9% around the Curie temperature, T_C, and ∼11% at 20 K. For all three curves, the resistance initially increases as the temperature is lowered, before reaching a maximum below which it decreases. This resistance maximum is generally found to occur close to T_C and the fall in resistance below T_C is attributed to suppression of spin-disorder scattering[19]. The position of the peak (Fig. 2, lower inset) changes from 91 K in accumulation to 85 K in depletion, with that of the reference bar between these values. This demonstrates that the polarization state of the gate significantly modulates the Curie temperature.

A higher degree of accuracy in inferring the Curie temperatures of (Ga,Mn)As materials can be achieved from the measured Hall resistivity, ρ_{xy}, which is dominated by the anomalous Hall component[23]. We have carried out measurements of ρ_{xy} and ρ_{xx}, the longitudinal resistivity, in magnetic fields perpendicular to the film, within the range of $-1.4\,T < B < 1.4\,T$. The ratio (ρ_{xy}/ρ_{xx}^n), with $n \sim 2$, is expected to track the magnetization, M for metallic materials, in the Berry-phase interpretation of the anomalous Hall resistivity[24]. T_C values can then be obtained from Arrott plots $((\rho_{xy}/\rho_{xx}^2)^2$ against $B/(\rho_{xy}/\rho_{xx}^2)$, where B is magnetic induction), because the ferromagnetic (paramagnetic) state corresponds to a positive (negative) intercept on the ordinate of the extrapolated linear behaviour at higher B values[23,25]. The Arrott plots, for $n = 2$, in accumulation and depletion, show clear shifts in the ordinate intercepts (Fig. 3a,b). This intercept is plotted versus T in Fig. 3c, from which T_C can then be read as the temperature at which the intercept passes through zero. This gives a Curie temperature that is ∼3.8 K (4.7%) lower in depletion than in accumulation (Fig. 3c). As the magnetic-field dependence of ρ_{xy} is much larger than that of ρ_{xx} for our samples, the shift in T_C obtained in this way is barely sensitive to the value of n: taking $n = 1$ (corresponding to the skew scattering picture[24]) gives a T_C shift of ∼3.2 K.

We now turn to the second structure, with a channel consisting of a (Ga,Mn)As film (II) without a (Al,Ga)As hole barrier. This structure shows qualitatively very similar trends for the temperature-dependent resistivities in the accumulation and depletion states compared to film I shown in Fig. 2; however, the resistance change is weaker by a factor 3. The shift of the resistance peak and the Arrott plot intercepts both indicate a control of T_C, with an intermediate resistance maximum and T_C in the Hall bar with the gate removed. The observed T_C shift of 1.8 K (2.2%) is weaker than in film I. This may be due in part to a higher carrier concentration in film II, consistent with the lower resistivity and/or the stronger confinement of holes (and hence smaller effective thickness) in the (Ga,Mn)As film I grown on the wider bandgap (Ga,Al)As material.

Table 1 summarizes the data on T_C shift driven by the ferroelectric gate. These measured T_C shifts are in good agreement with the predicted sublinear hole-concentration dependence $T_C(p)$ (ref. 26). From Table 1, the T_C shift associated with the resistance modulation in film I (II) gives $\partial(\ln T_C)/\partial(\ln R) \approx -0.5(-0.7)$. A detailed comparison can be made with the dependence on hole concentration of T_C and the conductivity as calculated microscopically within the kinetic-exchange model band structure and Boltzmann transport theory[27–29]. Within the model, a 6% Mn-doped film reaches T_C of 80 K for a hole concentration of

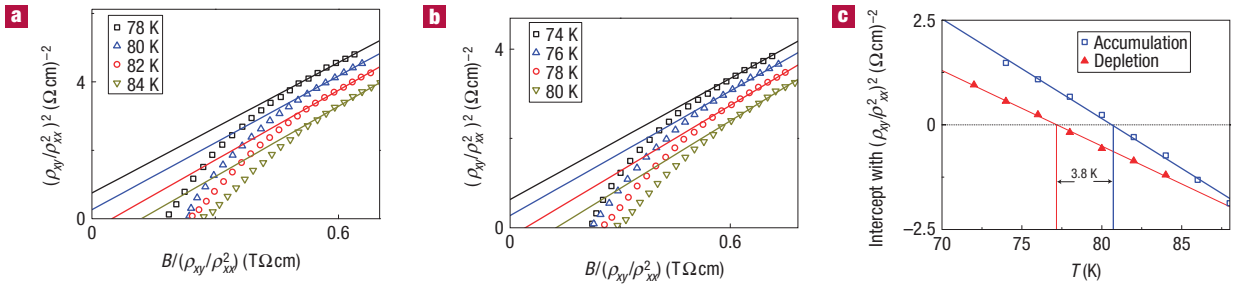

Figure 3 Control of ferromagnetism through ferroelectric switching: determination of the ferromagnetic T_C change by Arrott plots for film I. a,**b**, Arrott plots for the accumulation (**a**) and depletion (**b**). **c**, The intercepts from Arrott analysis plotted versus temperature, which give T_C of 76.9 K and 80.7 K, respectively, for depletion and accumulation.

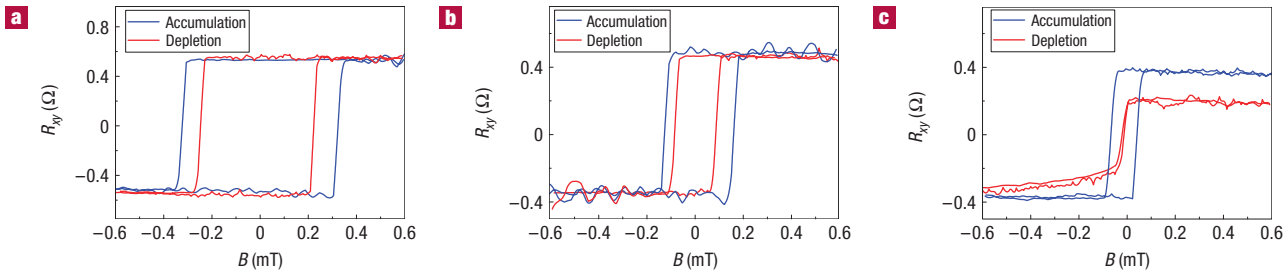

Figure 4 Control of ferromagnetism through ferroelectric switching: change of hysteretic properties by poling ferroelectric gate. a–c, The difference in the coercive field is clearly observed in the hysteresis loops of transverse resistance of film I plotted versus magnetic field for accumulation and depletion states for 50 K (**a**), 56 K (**b**) and 60 K (**c**). At 60 K, the hysteresis cannot be resolved in the depletion state, whereas in the accumulation state, it is still clearly observed.

Table 1 Change of sheet resistance and T_C shift induced by switching ferroelectric gate.

Sample	R (kΩ, accum.)	ΔR (kΩ)	T_C (K, accum.)	ΔT_C (K)
I	13.45	1.33 (9%)	80.7	3.8 (4.7%)
II	11.88	0.35 (2.9%)	84.1	1.9 (2.2%)

0.25×10^{21}cm^{-3}. Computed Curie temperatures for varying hole concentrations then indicate that $\partial T_C/\partial p = 2.15 \times 10^{-19}$ K cm^3 and $\partial(\ln T_C)/\partial(\ln p) = 0.68$. The calculated conductivity ($\sigma \propto 1/R$) is superlinear with $\partial(\ln R)/\partial(\ln p) = -1.4$, which then predicts $\partial(\ln T_C)/\partial(\ln R) = -0.48$, in agreement with our experimental data. Alternative Kubo formula calculations based on *ab initio*, coherent potential approximation band structures[30] predict $\partial(\ln T_C)/\partial(\ln R) \sim -0.6$ for the relevant Curie temperatures and resistivities, again in reasonable agreement with our experiments.

Hysteretic behaviour of the magnetization is another important signature of ferromagnetism, related to the magnetic anisotropy. We report a significant change of the hysteresis between accumulation and depletion states that clearly signals an altered magnetic state. Figure 4 shows hysteresis loops of transverse resistance of film I plotted as a function of magnetic field oriented along the Hall bar axis, which is within an accuracy of a few degrees the easy magnetization axis as determined from complementary superconducting quantum interference device measurements. Hysteresis is observed when the magnetization switches by ∼180° in the (001) plane. Note that we are able to observe this switch of magnetization as a change in transverse resistance due to an anomalous Hall signal that we ascribe to a small misalignment of ∼0.1° between the polished wafer plane (the Hall bar plane) and the magnetically easy (001) crystallographic plane. Such a misalignment is well within the quoted accuracy limits of the commercial substrates used. This interpretation is based on detailed measurements of the transverse magnetoresistance in out-of-plane and in-plane saturating magnetic fields. The dependence of the hysteresis on the gate voltage is clearly observed throughout the temperature range and becomes more pronounced when approaching T_C. The hysteresis cannot be resolved at 60 K in the depletion state and above 64 K in the accumulation state, consistent with a T_C difference of approximately 4 K.

Our results establish a number of important advances towards implementation of a FeFET multiferroic device. A widely recognized incompatibility between ferroelectrics and group III–V semiconductors has been solved by integration of a polymer ferroelectric in a FeFET configuration. Poling and retention in the polymer ferroelectric gate and electric-field control of ferromagnetism in the semiconductor channel have all been demonstrated successfully. The effects are in agreement with the established understanding of hole-mediated exchange in (Ga,Mn)As. In future, the gating efficiency may be enhanced by improved control of the polymer/semiconductor interface, for example by native oxide removal[31] to suppress detrimental screening effects at the polymer/(Ga,Mn)As interface. Other recent complementary studies on backgated (Ga,Mn)As structures with built-in low-voltage normal gates or bonded piezoelectric transducers[31,32] are also readily compatible with our FeFET structure. This opens new avenues for fundamental condensed-matter studies in cutting-edge areas such as collective

phenomena in systems with strong spin–orbit coupling or studies of quantum-relativistic transport and spin dynamics effects. Equally broad use is expected in applied research in new multifunctional device concepts for programmable logic, integrated information storage and retrieval, simultaneous non-volatile electrical, magnetic and mechanical (piezoelectric) gating, and of any combination of these functionalities in one physical element.

Received 20 December 2007; accepted 4 April 2008; published 4 May 2008.

References

1. Ramesh, R. & Spaldin, N. A. Multiferroics: Progress and prospects in thin films. *Nature Mater.* **6**, 21–29 (2007).
2. Eerenstein, W., Mathur, N. D. & Scott, J. F. Multiferroic and magnetoelectric materials. *Nature* **442**, 759–765 (2006).
3. Cheong, S. W. & Mostovoy, M. Multiferroics: A magnetic twist for ferroelectricity. *Nature Mater.* **6**, 13–20 (2007).
4. Ahn, C. H. *et al.* Electrostatic modification of novel materials. *Rev. Mod. Phys.* **78**, 1185–1212 (2006).
5. Wu, T. *et al.* Observation of magnetoelectric effect in epitaxial ferroelectric film/manganite crystal heterostructures. *Phys. Rev. B* **73**, 134416 (2006).
6. Wan, J. G., Liu, J. M., Wang, G. H. & Nan, C. W. Electric-field-induced magnetization in Pb(Zr,Ti)O-3/Terfenol-D composite structures. *Appl. Phys. Lett.* **88**, 182502 (2006).
7. Dorr, K. & Thiele, C. Multiferroic bilayers of manganites and titanates. *Phys. Status Solidi B* **243**, 21–28 (2006).
8. Srinivasan, G. *et al.* Structural and magnetoelectric properties of MFe_2O_4-PZT (M = Ni, Co) and $La_{-x}(Ca, Sr)_{(1-x)}MnO_3$-PZT multilayer composites. *Appl. Phys. A* **78**, 721–728 (2004).
9. Kanki, T., Tanaka, H. & Kawai, T. Electric control of room temperature ferromagnetism in a $Pb(Zr_{0.2}Ti_{0.8})O_{-3}/La_{0.85}Ba_{0.15}MnO_3$ field-effect transistor. *Appl. Phys. Lett.* **89**, 242506 (2006).
10. Zhao, T. *et al.* Electric field effect in diluted magnetic insulator anatase Co:TiO_2. *Phys. Rev. Lett.* **94**, 126601 (2005).
11. Venkatesan, T., Kundaliya, D. C., Wu, T. & Ogale, S. B. Novel approaches to field modulation of electronic and magnetic properties of oxides. *Phil. Mag. Lett.* **87**, 279–292 (2007).
12. Dietl, T. & Ohno, H. Engineering magnetism in semiconductors. *Mater. Today* **9**, 18–26 (2006).
13. Ohno, H. *et al.* Electric-field control of ferromagnetism. *Nature* **408**, 944–946 (2000).
14. Chiba, D., Yamanouchi, M., Matsukura, F. & Ohno, H. Electrical manipulation of magnetization reversal in a ferromagnetic semiconductor. *Science* **301**, 943–945 (2003).
15. Nazmul, A. M., Kobayashi, S., Sugahara, S. & Tanaka, M. Electrical and optical control of ferromagnetism in III–V semiconductor heterostructures at high temperature (similar to 100 K). *Jpn. J. Appl. Phys. Part 2* **43**, L233–L236 (2004).
16. Boukari, H. *et al.* Light and electric field control of ferromagnetism in magnetic quantum structures. *Phys. Rev. Lett.* **88**, 207204 (2002).
17. Park, Y. D. *et al.* A group-IV ferromagnetic semiconductor: Mn_xGe_{1-x}. *Science* **295**, 651–654 (2002).
18. Chiba, D., Matsukura, F. & Ohno, H. Electric-field control of ferromagnetism in (Ga,Mn)As. *Appl. Phys. Lett.* **89**, 162505 (2006).
19. VanEsch, A. *et al.* Interplay between the magnetic and transport properties in the III–V diluted magnetic semiconductor $Ga_{1-x}Mn_xAs$. *Phys. Rev. B* **56**, 13103–13112 (1997).
20. Naber, R. C. G. *et al.* High-performance solution-processed polymer ferroelectric field-effect transistors. *Nature Mater.* **4**, 243–248 (2005).
21. Rushforth, A. W. *et al.* AMR and magnetometry studies of ultra thin GaMnAs films. *Phys. Status Solidi C* **3**, 4078–4081 (2006).
22. Stolichnov, I. *et al.* Unusual size effect on the polarization patterns in micron-size $Pb(Zr, Ti)O_3$ film capacitors. *Appl. Phys. Lett.* **80**, 4804–4806 (2002).
23. Matsukura, F., Ohno, H., Shen, A. & Sugawara, Y. Transport properties and origin of ferromagnetism in (Ga,Mn)As. *Phys. Rev. B* **57**, R2037–R2040 (1998).
24. Jungwirth, T., Niu, Q. & MacDonald, A. H. Anomalous Hall effect in ferromagnetic semiconductors. *Phys. Rev. Lett.* **88**, 207208 (2002).
25. Arrott, A. Criterion for ferromagnetism from observations of magnetic isotherms. *Phys. Rev.* **108**, 1394–1396 (1957).
26. Jungwirth, T. *et al.* Prospects for high temperature ferromagnetism in (Ga,Mn)As semiconductors. *Phys. Rev. B* **72**, 165204 (2005).
27. Jungwirth, T., Abolfath, M., Sinova, J., Kucera, J. & MacDonald, A. H. Boltzmann theory of engineered anisotropic magnetoresistance in (Ga,Mn)As. *Appl. Phys. Lett.* **81**, 4029–4031 (2002).
28. Jungwirth, T., Konig, J., Sinova, J., Kucera, J. & MacDonald, A. H. Curie temperature trends in (III,Mn)V ferromagnetic semiconductors. *Phys. Rev. B* **66**, 012402 (2002).
29. Jungwirth, T., Sinova, J., Masek, J., Kucera, J. & MacDonald, A. H. Theory of ferromagnetic (III,Mn)V semiconductors. *Rev. Mod. Phys.* **78**, 809–864 (2006).
30. Kudrnovsky, J., Bouzerar, G. & Turek, I. Relation of Curie temperature and conductivity: (Ga,Mn)As alloy as a case study. *Appl. Phys. Lett.* **91**, 102509 (2007).
31. Olejnik, K. *et al.* Enhanced annealing, high Curie temperature and low-voltage gating in (Ga,Mn)As: A surface oxide control study. Preprint at <http://arXiv.org/abs/0802.2080> (2008).
32. Rushforth, A. W. *et al.* Voltage control of magnetocrystalline anisotropy in ferromagnetic-semiconductor/piezoelectric hybrid structures. Preprint at <http://arXiv.org/abs/0801.0886> (2008).

Acknowledgements

We acknowledge support from the Swiss National Science Foundation; Swiss Program on NanoSciences (NCCR); EU Grant IST-015728, UK Grant GR/S81407/01; CR Grants FON/06/E002, AV0Z1010052, KAN400100652 and LC510; US NRI Grant SWAN.

Author information

Reprints and permission information is available online at http://npg.nature.com/reprintsandpermissions. Correspondence and requests for materials should be addressed to I.S.